Journal of Hazardous Materials 516 (2026) 143415

Contents lists available at ScienceDirect

Journal of Hazardous Materials

journal homepage: www.elsevier.com/locate/jhazmat

Quantitative classification of asbestos-like morphology for assessing potentially hazardous fibrous minerals

Jasmine R. Petriglieri [a,b], Luca Barale [a,c], Maura Tomatis [a,d], Alessandro Cavallo [e], Chiara De Giuli [a,f], Maria Rosaria Bruno [g], Angelo Olori [h], Biagio Maria Bruni [i], Paolo Ballirano [j], Elena Belluso [a,b], Fabrizio Piana [a,c], Alessandro Pacella [j], Antonella Campopiano [h], Francesco Turci [a,f,*]

[a] "G. Scansetti" Interdepartmental Centre for Studies on Asbestos and Other Toxic Particulates, University of Torino, Via Pietro Giuria 9, Torino I-10125, Italy
[b] Department of Earth Sciences, University of Torino, Via Valperga Caluso 35, Torino I-10125, Italy
[c] Institute of Geosciences and Earth Resources, National Research Council (CNR) of Italy, Torino, Italy
[d] Department of Veterinary Sciences, University of Torino, Largo Paolo Braccini 2, Grugliasco, Torino I-10095, Italy
[e] Department of Earth and Environmental Sciences, University of Milano-Bicocca, Piazza della Scienza 4, Milano I-20126, Italy
[f] Department of ChemistryUniversity of Torino, Via Pietro Giuria 7, Torino I-10125, Italy
[g] Department of Medicine, Epidemiology, Occupational and Environmental Hygiene, National Institute for Insurance against Accidents at Work (INAIL), Zona Industriale Benedetto XVI, Lamezia Terme 88046, Italy
[h] Department of Medicine, Epidemiology, Occupational and Environmental Hygiene, National Institute for Insurance against Accidents at Work (INAIL), via Fontana Candida 1, Monte Porzio Catone, Rome 00078, Italy
[i] Department of Environment and Health, National Health Institute (ISS), Rome, Italy
[j] Department of Earth Sciences, Sapienza University of Rome, Piazzale Aldo Moro 5, Rome I-00185, Italy

HIGHLIGHTS

- Fibrosity parameter quantifies asbestos-like fragmentation behaviour.
- Fp combines EMP_{20}% and EMP stability under controlled milling.
- Fp distinguishes retained from progressively lost fibrosity.
- Macroscopically elongated tremolite showed non-asbestos-like morphology.
- Quantitative workflow supports morphological screening of fibrous minerals.

GRAPHICAL ABSTRACT

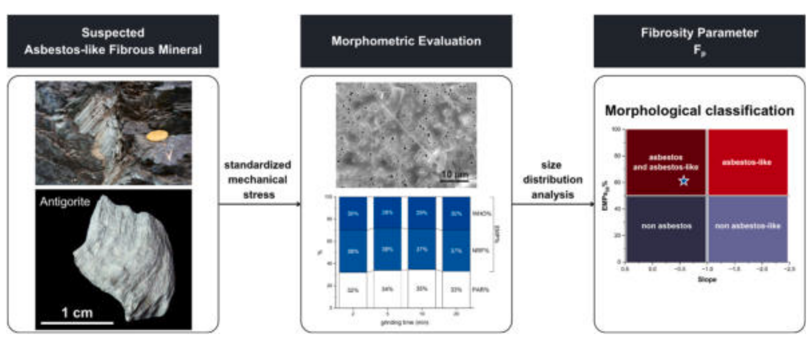

ARTICLE INFO

Keywords:
Naturally occurring asbestos
Elongate mineral particles
Antigorite

ABSTRACT

Hazard assessment of naturally occurring asbestos and asbestos-like minerals (NOA) is hindered by the lack of standardized criteria for quantifying asbestos-like morphology. This work introduces the fibrosity parameter (F_p), an experimental approach for classifying suspected fibrous minerals. F_p combines standardized mechanical stress with automated morphometric analysis to evaluate changes in the percentage of elongate mineral particles

* Corresponding author at: "G. Scansetti" Interdepartmental Centre for Studies on Asbestos and Other Toxic Particulates, University of Torino, Via Pietro Giuria 9, Torino I-10125, Italy.
E-mail address: francesco.turci@unito.it (F. Turci).

https://doi.org/10.1016/j.jhazmat.2026.143415
Received 13 May 2026; Received in revised form 27 July 2026; Accepted 26 August 2026
Available online 27 August 2026

Tremolite
Morphometry
Fibrosity
Hazard assessment

(EMP) during milling. The approach was tested on five antigorite and three tremolite samples spanning fibrous, lamellar, and prismatic morphologies, using crocidolite, amosite, MMVF, and talc as references. F_p is defined by EMP% after 20 min of milling (EMP_{20}%) and the slope of EMP% between 2 and 20 min (S). Thresholds of $EMP_{20}\% = 50\%$ and $S = -1$ distinguished four morphological scenarios: 1) asbestos or asbestos-like, 2) precautionary asbestos-like, 3) non-asbestos-like, and 4) non-asbestos. Fibrous antigorite samples and one tremolite retained high EMP contents and behaved comparably to asbestos references, whereas another macroscopically fibrous tremolite progressively lost fibrosity and was classified as non asbestos-like. Thus, macroscopic fibrosity is not a reliable proxy for asbestos-like fragmentation behaviour. F_p provides a quantitative and reproducible morphological screening tool that complements broader hazard assessment. However, F_p is not a stand-alone predictor of pathogenicity.

1. Introduction

The widespread occurrence of naturally occurring asbestos (NOA) globally demands an advanced geological hazard evaluation to establish health protection from asbestos during large infrastructure projects [1–5]. The term NOA is used to distinguish naturally occurring asbestos and asbestos-like minerals from the term "asbestos", which specifically defines only six commercially-relevant mineral fibres (i.e., chrysotile, crocidolite, amosite, anthophyllite asbestos, actinolite asbestos, and tremolite asbestos) that were widely employed in the past century and are responsible for the most severe occupational epidemic in human history [6–10]. NOA are rock and soil forming minerals in mafic and ultramafic rocks, as the result of natural geological processes [11–13]. From the point of view of hazard evaluation, NOA includes hazardous fibrous minerals (e.g., fuoroedenite, erionite, and winchite) which share with asbestos some key physico-chemical properties relevant for toxicity, including an asbestos-like morphology, but that do not strictly comply with regulatory definitions of asbestos derived from commercially available fibres ([13]; EU Directive 2023/2668/EC). For instance, NOA may show a chemical composition or a mineral structure that differs from that of the six phases identified as asbestos and yet the exposure to those minerals might represent a hazard for humans [14–18]. Human activities (e.g., construction of infrastructure) and natural processes (e.g., erosion, weathering) may disturb and mobilize fibres, thus posing a risk for human health and the environment. The emergence of asbestos-related diseases associated with non-industrial exposure (e.g., [19–25]) requires updating hazard assessment, monitoring, and mitigation strategies in these emerging scenarios [26,27]. The largely unexplored impact of exposure to NOA prompted the European Parliament to pass a resolution that aims to raise awareness of the social and health implications of their occurrence in large areas of several European countries ([28]; 2019/2182(INL)). In this context, the natural occurrence of several asbestos-like minerals may pose a risk to workers and the residential population, but the lack of proper tools to evaluate their hazard dramatically impairs the enforcement of effective safety procedures (e.g., [29–31]).

The identification of the asbestos morphology of fibre bundles and individual fibres in bulk industrial and commercial materials, commonly referred to as Asbestos-Containing Materials (ACMs), is widely regulated by environmental, health and safety agencies (e.g., US Environmental Protection Agency, World Health Organization, International Agency for Research on Cancer). The United States Environmental Protection Agency (EPA) and the World Health Organization (WHO) defined asbestos respirable fibres as particles which may present the following characteristics: i) length $L > 5$ μm, width $W < 3$ μm, and length to width ratio > 3 (aspect ratio, AR=L/W; WHO 1997 counting criteria [32]); ii) high or extremely high aspect ratios, ranging from 10:1–100:1 or higher; iii) very thin individual fibres, usually less than 0.5 μm in width; iv) high curvature and flexibility; v) parallel fibres occurring in bundles characterised by splayed ends (EPA, 1993; ISO 10312:2019; WHO 1997 [32-34]). It is worth noting that not all five of these parameters are strict morphological properties of the mineral that can be objectively assessed during analysis. In 2011, the NIOSH introduced the term Elongate Mineral Particles (EMP), expanding the dimensional boundaries of "asbestos respirable fibre" to all the potentially hazardous elongate mineral particles with AR > 3 and length > 5 μm (NIOSH, 2011 [35]). However, such standardized and harmonized procedures are currently lacking for NOA.

To classify NOA in the context of their potential hazard, a quantitative parameter to express the fibrosity of a suspected hazardous EMP is needed ([36–39] and references therein). In recent years, increasing attention has been devoted to linking the morphometry of EMP with pathological outcomes [40–43], although these approaches remain largely focused on industrial asbestos and do not adequately address the complexity of NOA. Several mathematical approaches have been reported in the literature to investigate the asbestos morphological behaviour of industrial asbestos. Most of these works aim to establish quantitative relationships between airborne asbestos characteristics (exposure or inhalation indexes) and health outcomes, particularly the risk of developing asbestos-related diseases such as mesothelioma and lung cancer. Large databases incorporating key dimensional parameters (length, width, and AR), along with data from epidemiological and toxicological studies, were analysed using descriptive statistics, correlation and regression analysis, and Monte Carlo simulation to develop mathematical algorithms for predicting the carcinogenic potency of airborne asbestos ([41] and references therein). A pioneering attempt to develop a mathematical index (i.e., fibrosity index) for the discrimination of asbestos habit based on fibre length and width measurements was performed on a set of commercially milled asbestos minerals by Siegrist and Wylie, (1980) [44]. Later, different procedures complementing or overcoming the aspect ratio (e.g., [44–49]) and the width [13,40,43] criteria have been proposed by the scientific community. These studies confirm dimensions as one of the main drivers of asbestos carcinogenicity [50].

A mathematical framework for estimating the asbestos-like morphology of NOA, consisting of the size and distribution, remains undeveloped. Currently available approaches often take an overly simplistic approach to describing the minerals' morphometric parameters, relying mainly on the average length and diameter of a heterogeneous population of fibrils, fibres, and bundles. In the Fibre Potential Toxicity Index (FPTI), an empirical model for predicting the toxicity of a mineral fibre, the mean length and diameter of a preparation of the unknown mineral are used as two of the key parameters governing the overall mineral toxicity, jointly with surface reactivity and dissolution rate [36,51]. However, this approach does not account for the variability and spread of the particle population. In the realm of NOA, the average dimensions of a possible asbestos-like mineral are evaluated after a non-standardized comminution process of a hopefully pure vein of a single mineral phase. Mechanical comminution of both massive and asbestos-like minerals produces a continuous range of particle habits and sizes [52], generating heterogeneous particle populations in which critical subpopulations may be overlooked when only mean values are considered. Militello et al. (2020, 2021) demonstrated that grinding both non-asbestos and asbestos-like amphiboles, specifically massive tremolite and tremolite asbestos, can generate a spectrum of particles and EMPs [53–55], but neither the comminution method nor grinding time substantially alters the predominant asbestos-like morphology. Thus, the aspect ratio remains largely unaffected by external processing, even if the individual distributions of length and width are influenced [43,56].

The definition of asbestos-like morphology in mineral fibres is not unambiguous or performed under harmonized procedures. Assessing whether a naturally occurring mineral that displays a fibrous morphology at the macroscopic scale also exhibits an asbestos-like morphology at the microscopic level is a significant challenge for the analyst and a dramatic source of uncertainties in geological hazard of natural sites [53,55]. While a mineral may appear fibrous and characterised by elongated lamellar, acicular or needle-like structures when observed with the naked eye or low magnification, it might not possess the distinct morphometric properties that define asbestos-like fibres. Although a comprehensive morphological definition of asbestos is still under debate [57], it is largely held that asbestos minerals consist of bundles of long and thin particles that exhibit poly-filamentous behaviour. Asbestos minerals preferentially split along their growth axis, which results in the formation of long and thin fibres (i.e., fibres with high aspect ratio; IARC 2012 [58]). This peculiar morphology, here referred to as asbestos-like morphology, persists even under strong mechanical stress (e.g., comminution; [55,59]). Indeed, asbestos fibres are generated through a crystal growth mechanism that is clearly recognized by the mineralogical community but does not include clear morphometric boundaries [43]. Applying an increasing mechanical stress on non-asbestos fibrous minerals will promote the cleavage of elongated particles into isometric particles. Generally, non-asbestos fibrous minerals split perpendicularly to the growth direction and generate the so-called "cleavage fragments" [60]. This mechanism implies the loss of the fibrosity of non-asbestos minerals, even when they show a clear fibrous morphology at the macroscopic scale. On this basis, different conceptual fragmentation behaviours may be distinguished. Mineral occurrences may either retain a high proportion of elongated particles under progressive mechanical stress, displaying an asbestos-like morphology, or they may predominantly generate isometric particles, displaying a non-asbestos morphology. Intermediate behaviours include initially populations that progressively lose elongated particles during milling and populations that retain a high EMP content despite a measurable decrease in fibrosity. The partial overlap between EMPs, cleavage fragments, and regulated asbestos and asbestos-like fibres commonly occurs in scientific literature and laboratory practice, further complicating the identification and classification of hazardous fibres.

This work introduces the "Fibrosity parameter (F_p)" to quantitatively evaluate the asbestos-like morphology of a suspected fibrous mineral in natural sites. A protocol was therefore designed to verify whether a mineral that is suspected to have asbestos-like properties preserved its fibrous morphology after a standardized mechanical stress, such as milling. The particle and fibre length and width size distribution were estimated by means of light microscopy coupled with automated image analysis (FPIA) and Scanning Electron Microscopy (SEM). This multi-technique approach allows thousands of particles to be measured with respect to SEM investigation alone, providing a reliable statistical analysis to comparatively classify minerals under investigation. F_p was evaluated on a set of antigorite and tremolite samples showing a fibrous to lamellar/prismatic morphology at the macroscopic scale. Data on investigated minerals were compared with data obtained with asbestos and non-asbestos standards, i.e., UICC crocidolite and amosite, and Man Made Vitreous Fibres (MMVF) and talc. A quantitative assessment of the asbestos-like morphology of the minerals was proposed.

F_p offers a practical, reproducible approach that laboratories could easily adopt for screening and monitoring purposes. Its implementation would support a more quantitative classification of asbestos-like morphology of a suspected mineral fibre, complementing current morphological assessments towards hazard analysis.

2. Materials and methods

2.1. Materials

A set of five macroscopically lamellar-to-fibrous antigorite and three macroscopically prismatic-to-fibrous tremolite samples were investigated in this study. The potential asbestos-like morphology was compared with the asbestos morphology of UICC Crocidolite [61] and long amosite [52,62], and with the non-asbestos morphology of Man Made Vitreous Fibres (MMVF10; [63]) and lamellar talc from the Fontane deposit, hosted in pre-Carboniferous rocks of the Dora-Maira Massif (Western Alps, Italy; [64]).

2.1.1. Antigorite samples

Antigorite samples were collected from veins in i) antigorite serpentinite of Palmaro-Caffarella Unit, Voltri Massif (Atg-1, Atg-2, Atg-5) (Varenna Valley, Liguria, Italy; [65]); ii) antigorite serpentinite of Gimigliano-Monte Reventino Unit, Southern Ligurian Domain (Atg-3) (San Mango d'Aquino, Calabria, Italy; [56]); and iii) weathered antigorite serpentinite of Koniambo Massif, Peridotite Nappe (Atg-4) (Tontouta, Nouvelle-Calédonie, France; [15].

2.1.2. Tremolite samples

Tremolite samples were from: i) a vein in antigorite serpentinite of Cerogne-Ciantiplagna Unit, External Piemonte Zone (Trm-1) (Sauze d'Oulx, Piemonte, Italy; [66]; ii) a vein in a talc-chlorite-schist mass included within the antigorite serpentinite of the Internal Piemonte Zone (Trm-2) (Bracchiello abandoned quarry, Ceres, Piemonte, Italy; [67]); and iii) dolomitic marble of Campolungo Zone, Simano Nappe, Lower Penninic Units (Trm-3) (Campolungo, Ticino, Switzerland; [68].

Samples differ macroscopically from fibrous (Atg-1, Atg-2, Atg-3, Atg-4, Trm-1, Trm-2) to non-fibrous lamellar or prismatic morphology (Atg-5, Trm-3). Mesoscale features of antigorite veins and fragments embedded in their host rocks are reported in Supplementary Materials (S1). The mineralogical identification of the selected vein fragments was preliminarily assessed using X-ray powder diffraction (XRPD), micro-Raman spectroscopy, and scanning electron microscopy (SEM), and representative results for each sample are reported in the Supplementary Materials (S2).

2.2. Methods

2.2.1. X-ray powder diffraction (XRPD)

The bulk mineralogy was determined by qualitative XRPD analysis using a Rigaku Miniflex 600 diffractometer. Intensity measurements were run at 40 kV and 15–40 mA, using CuKα radiation (λ = 1.54178 Å) over a 2θ range from 3 to 90∘ 2θ in steps of 0.02∘, with a counting time of 1 s per step. The limit of detection of XRPD depends on the mineral phase and is usually 1 wt% for crystalline secondary and accessory phases, and 5 wt% for serpentine and amphibole minerals. Representative diffraction patterns of each antigorite and tremolite sample are reported in Supplementary Materials S2.

2.2.2. Micro-Raman spectroscopy

Raman spectra were obtained with a Horiba HR800 Raman spectrometer equipped with an Olympus BX41 confocal microscope, a 600-grooves/mm holographic grating monochromator, and a high-gain Peltier-cooled CCD. A Nd solid state laser at 532-nm was used as excitation, and neutral density filters were used to avoid sample heating. Up to 15 spectra were obtained on vein fragments using a 10× objective. The spectrometer was calibrated using the 520.7 cm^{-1} Raman peak of silicon before each experimental session. Spectra were collected as follows: 6 acquisitions for 20 s in the low and high wavenumber spectral range were averaged and background-subtracted with LabSpec® software. Representative Raman spectra of each antigorite and tremolite sample are reported in Supplementary Materials S2.

2.2.3. Ball mill grinding

A fixed aliquot of the < 2 mm fraction (1.8 g) was dry ground in a ball mixer mill (Retsch MM200) for 2, 5, 10, and 20 min at 27 Hz using an agate jar (15 mL) with 4 agate balls (5 mm diameter).

2.2.4. Flow particle image analysis (FPIA)

Particle size distribution of comminuted specimens in a range of 0.8–300 μm was obtained by Flow Particle Image Analysis (FPIA) using the Sysmex FPIA-3000 apparatus (Malvern Instruments). Specimen powders were dispersed in ultrapure water (0.5 mg/mL) and sonicated for 30 s at 10 W. Each suspension was passed through a cell where images of particles were captured using stroboscopic illumination and a CCD camera (20× magnification lens). Particles with a Circular Equivalent Diameter (CED) of less than 4 μm were excluded from counting. The CED 4 μm threshold was selected based on the instrumental detection limit. Because CED is the diameter of the circle having the same projected area as the particle image, CED threshold of 4 μm does not correspond to the measured Length and Width. According to $A = \pi CED^2/4$, a CED of 4°μm corresponds to a projected area of approximately 12.57 μm^2. The criterion may therefore exclude particles with small projected areas, particularly short and thin particles, but does not systematically remove all particles with submicrometric widths. Removing particles below a particular size threshold, consisting of high numbers of low-volume particles, reduces the risk of under-sampling high-volume particles whilst having minimal effect on the overall geometric distribution of powder samples [69]. Particle dimensions were quantified as length (L), defined as the length of the longer axis of the particle image when bounded by two pairs of parallel lines, and width (W), defined as the length of the shorter axis under the same conditions. Data were evaluated and plotted using OriginPro Software (Adalta, Italy).

2.2.5. Scanning electron microscopy (SEM)

Secondary Electron (SE) and Backscattered Electron (BSE) images were acquired at 10–15 kV, 100 pA by Scanning Electron Microscope (SEM) TESCAN VEGA 4 equipped with an Oxford Ultim Max 40 EDS.

Preliminary morphological analyses were performed on representative vein fragments mounted on aluminium stubs using conductive carbon adhesive tabs and gold-coated. BSE images were acquired at about 100x, 750x and 3000x magnification (Field of View, FOV 3490, 558, and 140 μm, respectively; image dimension 1024 ×1024 px).

Quantitative morphometric analyses were subsequently performed on the milled powder samples. The sample preparation procedure was adapted from ISO 14966:2019 [74]. Approximately 5 mg of each specimen powder was weighed and suspended in an aqueous solution containing 0.1% surfactant. A known volume of the suspension was filtered through a polycarbonate membrane filter (25 mm diameter; 0.8 μm pore size) to obtain a deposited powder mass of approximately 0.01–0.1 mg. The filters were then dried and gold-coated. SE images were collected at 2500x magnification (FOV 112 μm; image dimension 1024 ×1024 px; pixel size 0.109 μm px-1).

3. Results

3.1. The fibrosity analytical approach

The analytical approach for determining the “fibrosity parameter” aims to assign a morphological classification to a specific mineral occurrence to evaluate its asbestos-like nature. Although asbestos minerals cannot be defined solely based on morphological data, a necessary condition is that the fibres can split almost indefinitely along crystallographic planes parallel to the crystal growth axis. Given that potentially fibrous minerals occur in nature with a wide diversity of morphologies and structural features, we have developed a quantitative approach to assess whether a mineral exhibits fragmentation behaviours morphologically comparable to that of asbestos. The approach involves five main steps: i) preliminary sample preparation for subsequent milling; ii) standardized progressive mechanical stress; iii) morphometric analysis; iv) data analysis; and v) obtaining the fibrosity parameter (F_p). The experimental setup is schematically illustrated in Fig. 1.

i. *Sample preparation*. This step is devoted to producing powder specimens that are representative in both mass and particle size. Vein samples were collected from natural outcrops by hand-picking with tweezers after gently removing the superficial portion of the potentially weathered material. A fixed aliquot of vein fragments (10 g) was gently hand-crushed and sieved to obtain a homogenous size fraction < 2 mm. Statistically relevant mass and size reduction steps were carried out by applying the approach adapted to NOA by Turci et al. (2020) [70], derived from Pierre Gy’s theory ([71] and therein).
ii. *Standardized mechanical stress*. It consists of a controlled ball milling procedure at multiple time points in the 2–20 min range. The fraction < 2 mm was ground following the comminution procedure (see par. 2.2.3) for 2, 5, 10, and 20 min (from t_2 to t_{20}). The shorter time (2 min) induced a gentle material separation, producing fibres and particles that could be analysed by electron microscopy. The protocol was previously validated for antigorite and tremolite samples for toxicological assays (e.g., [15]). The 2 min time point was selected as the initial stage of milling kinetics. The morphometric data obtained were analysed to characterize particle populations in terms of mineral morphology and size distribution. The following time points produced a further reduction of the particle dimensions. Furthermore, the milling procedure was designed to be carried out in a relatively reasonable amount of time, making the implementation of this approach feasible in any conventional analytical lab. After grinding, powder samples were sieved at 300 μm to refine the size range of the samples and to remove, if present, larger particles that exceeded the upper limit of detection of light and electron microscopy.
iii. *Morphometric evaluation*. Particle shape and particle size distribution of powdered samples in a range of 0.8–300 μm were obtained by optical light microscopy coupled with an automated image analysis (FPIA). More than 1500 individual particles were analysed for each specimen (Supplementary Materials, S3).

   Scanning electron microscopy was used to confirm the reliability of the automated morphometric evaluation carried out with FPIA. Length, width, and AR of 300 individual particles were measured for the two endpoint grinding times (t_2 and t_{20}) for each sample (Supplementary Materials, S5). The mean difference between methods was minimal (-0.09) and most data points fell within the 95% limits of agreement.
iv. *Data analysis*. The morphometric data obtained were analysed to characterize particle populations in terms of particle morphology and size distribution. Concerning counting criteria, in this work, we adopted the morphometric definition of particles and elongated mineral particles introduced in Petriglieri et al. (2023) [65]. Specifically, we defined:

– particles (PAR), any non-elongated mineral particle that has a length to width ratio (AR) lower than 3;
– elongated mineral particle (EMP), any mineral particle with a length to width ratio (AR) greater than 3. AR is defined assuming the width of a particle to be an apparent parameter defined as the longest dimension of the particle in the plane perpendicular to the length and the shortest dimension of the two-dimensional outline of a particle (according to [35] and Report IMA 2022 [72]);
– non-respirable fibre (NRF), any EMP with a length greater than 5 μm and a width greater than 3 μm;
– respirable WHO fibre (WHO), any EMP that has a length greater than 5 μm and a width lower than 3 μm. This definition is consistent with

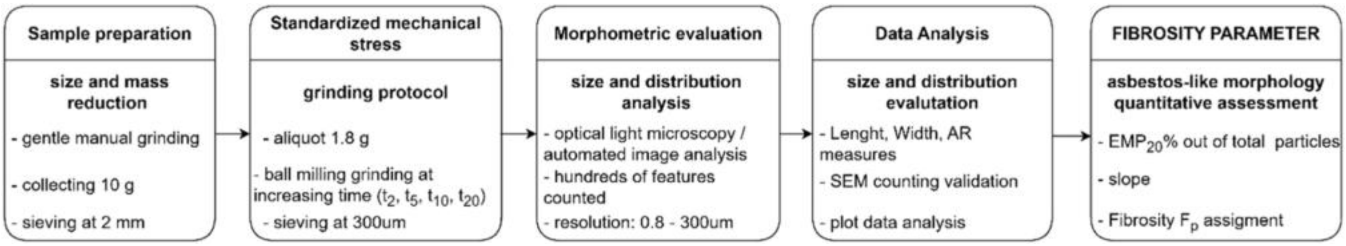

Fig. 1. Experimental set-up scheme of the analytical protocol designed to calculate F_p, the fibrosity parameter to describe the asbestos-like morphology of a suspected fibrous mineral.

the counting criteria proposed by WHO (1997) for the determination of airborne asbestos fibres in occupational monitoring.

v. *"Fibrosity parameter (F_p)"*. F_p classifies the morphology of suspected fibrous minerals by considering two criteria: 1) the percentage of EMP out of the total features detected at t_{20} (EMP_{20}%); and 2) the slope of the linear regression interpolating the EMP% at the four timepoints (EMP_2%, EMP_5%, EMP_{10}%, and EMP_{20}%).

3.2. Morphological description of antigorite and tremolite vein fragments at the macroscale

At the macroscopic scale, antigorite and tremolite vein fragments displayed a range of appearances, from markedly fibrous and predominantly splintery (Atg-1, Atg-2, Atg-3, Atg-4, Trm-1, Trm-2) to massive (Atg-5 and Trm-3). Their colours varied from green blue (Atg-2, Atg-3, Atg-5) to whitish (Atg-1, Atg-4, Trm-1, Trm-2, Trm-3), as illustrated in Fig. 2. Samples Atg-1, Atg-2, and Atg-3 showed a weak cohesion and flexible and noticeably friable aspect, dominated by elongated crystals cracking into thinner curvilinear laminas. Samples Atg-4, Trm-1, and Trm-2 showed a weak cohesion and occurred as centimetre-long bundles of parallel elongated lath- and acicular-shaped crystals presenting splayed or frayed ends. Sample Atg-5 and Trm-3 were cohesive and characterized by platy-shaped fabric of parallel blades or prismatic elongated crystals, respectively.

3.3. Morphometric evaluation

The dimensions, consisting of length L, width W, and AR parameters, of approximately 1500 mineral objects for each antigorite, tremolite and reference sample at increasing grinding times were measured by optical microscopy coupled with automated image analysis. Considering thousands of objects provided statistical confidence that the measurements adequately represented the distribution of powder samples.

The relative comparison of particles (PAR%; % of particles with AR <3 of total particles), elongated mineral particles (EMP%; % of particles with AR >3 of total particles) consisting of non-respirable fibres (NRF%; % of particles with AR >3, L >5 μm, and W >3 μm of total particles), and respirable WHO fibres (WHO%; % of particles with AR >3; L >5 μm; W <3 μm of total particles; WHO 1997 counting criteria) populations, generated for each sample after milling procedure, is illustrated in Fig. 3.

Antigorite Atg-1, Atg-2, Atg-3 and Atg-4 exhibited WHO% and NRF% in the range 47–26% and 42–35%, respectively. On the other hand, they displayed PAR% in the range 11–34%. Antigorite Atg-5 showed a lower WHO% and NRF% (13–17% and 19–18%, respectively) and a higher PAR%, ranging from 68% to 64%. The stacked chart revealed that by increasing the grinding time (from t_2 to t_{20}), the EMP%, namely WHO fibres and non-respirable fibres, remained approximately constant % for sample Atg-1 and Atg-5, while we observed a slight decrease in EMP% for Atg-2, Atg-3, and Atg-4.

Tremolite Trm-1 exhibited WHO% and NRF% in the range 37–35% and 44–34%, respectively. The PAR% was in the range 20–31%. As expected, tremolite Trm-3 displayed a lower WHO% and NRF% content (9–6% and 20–16%, respectively) and a higher PAR% content, ranging from 71% to 77%. Trm-2, exhibiting very elongated structures at the macroscale, showed lower WHO% and NRF% (12–6% and 31–7%, respectively) and a higher PAR%, ranging from 57% to 87%. As grinding time increased, EMP% populations decreased slightly (Trm-1) to markedly (Trm-2) for fibrous tremolites, while it remained constant for prismatic non-fibrous tremolite (Trm-3).

For comparison, the % populations of milled MMVF (non-asbestos fibres) and talc (lamellar mineral) is also reported in Fig. 3. MMVF displayed WHO% and NRF% in the range 28–11% and 43–17%, respectively. PAR% was in the range 29–72%. Talc showed a small WHO % and NRF% content (5–3% and 12–9%, respectively) and a larger PAR % content, ranging from 84% to 88%. By increasing the grinding time, the EMP% populations dramatically decrease for non-asbestos fibres MMVF and slightly decrease for lamellar talc. As for the latter, cleavage of non-respirable fibres with milling is responsible for the slight decrease of EMP% (12–9%) and therefore with the increase of PAR%.

Representative SEM images reported in Fig. 3 displayed the morphology of samples at the endpoints t_2 and t_{20}. The automatic counting approach proposed was validated by SEM, measuring manually the dimension parameters of about 300 objects at t_2 and t_{20} of each sample (see Supporting Materials, table S4).

Particle and fibre size distributions of milled antigorite and tremolite samples were compared with asbestos (UICC crocidolite, amosite) and non-asbestos minerals (MMVF, talc), as shown in Fig. 4.

Fibrous antigorite (Atg-1, Atg-2, Atg-3, Atg-4) and fibrous tremolite (Trm-1) exhibited EMP% and WHO% ranging from 80% to 65% and 47–26% with increasing milling time, t_2 and t_{20} respectively. A slight but negligible decrease in fibrous morphology is observed. It is relevant to point out that most of the EMP detected had the dimensions of respirable WHO fibres (WHO, 1997). These samples preserved their fibrous morphology and fall in the range of fibrosity of asbestos. Asbestos UICC crocidolite and amosite displayed similar values in terms of EMP% (83% and 82%, respectively) and WHO% (47% and 58%, respectively).

Massive lamellar antigorite (Atg-5) and massive prismatic tremolite (Trm-3) preserved their lamellar/prismatic morphology, generating after t_{20} milling less than 35% of EMP% and less than 15% of WHO%, in accordance with non-asbestos lamellar mineral (EMP_{20}% = 12% for talc).

Although tremolite Trm-2 exhibited very elongated structures at the macroscopic scale, it rapidly lost its fibrous morphology with milling time. At minimum grinding time t_2, the EMP% and WHO% dropped at 42% and 12%, respectively. At the maximum milling time t_{20}, the EMP% and WHO% collapsed to 13% and 6%, respectively. A similar decreasing trend was observed for non-asbestos fibres MMVF (EMP% from 55% to 28% and WHO% from 28% to 11%).

The fibrosity behaviour of asbestos-tremolite (Trm-1) was clearly distinct from the fibrosity of tremolite, both prismatic (Trm-3) and fibrous non-asbestos (Trm-2). Likewise, the fibrosity of asbestos-like antigorite (Atg-1, Atg-2, Atg-3, Atg-4) was distinct from the fibrosity of lamellar antigorite (Atg-5). This separation is more noticeable considering the percentage of EMP (Fig. 4). A least-squares regression analysis was conducted to quantitatively describe these differences in

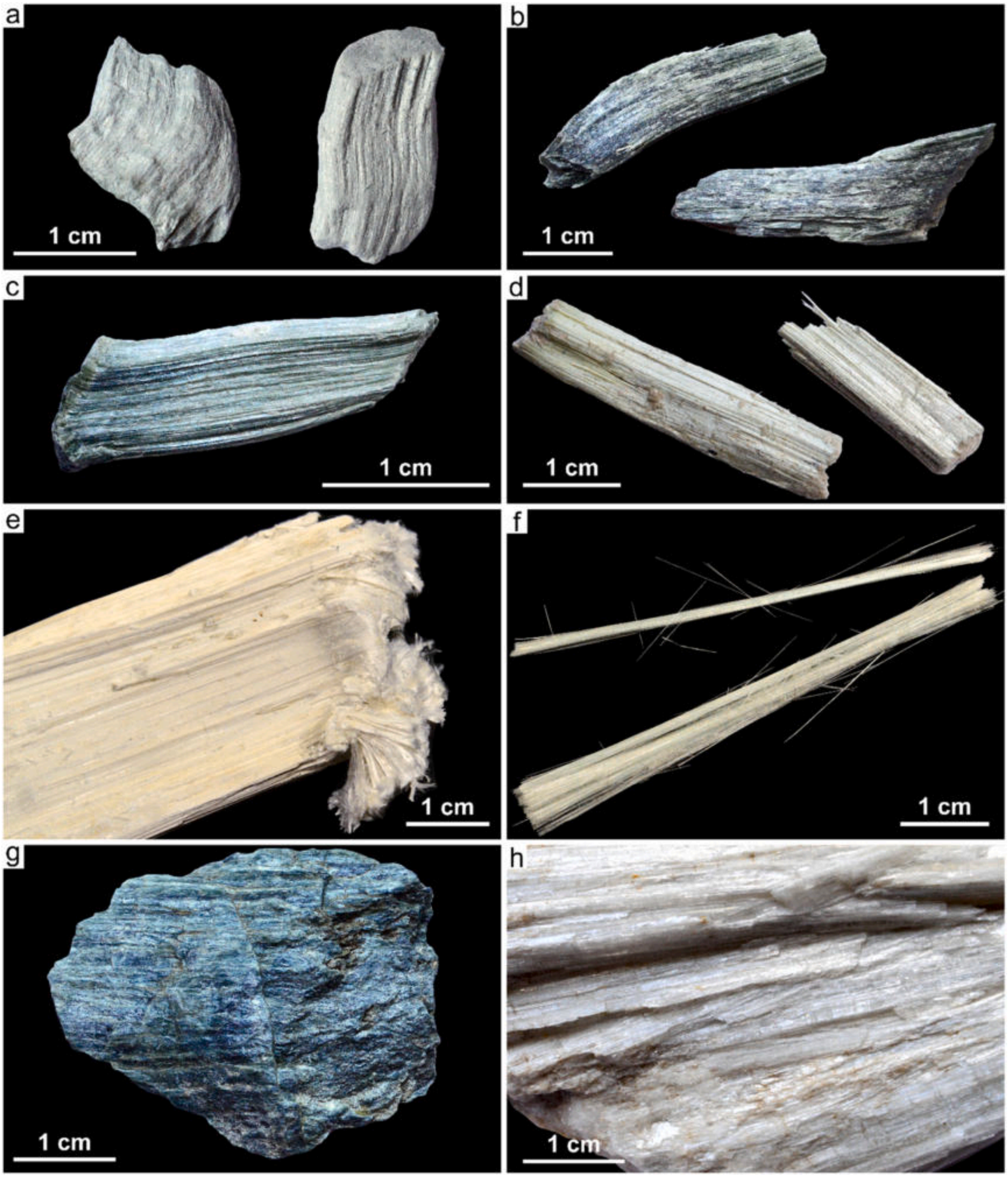

Fig. 2. Macroscopic description of the antigorite and tremolite specimens. The representative images illustrate the range of morphologies, from fibrous to non-fibrous lamellar/prismatic. a-b) fibrous antigorite from different veins in a NOA site in Varenna Valley (Atg-1 and Atg-2, respectively); c) fibrous antigorite from San Mango d'Aquino (Atg-3); d) fibrous antigorite from New Caledonia (Atg-4); e) fibrous tremolite from Sauze d'Oulx (Trm-1); f) fibrous tremolite from Bracchiello (Trm-2); g) massive lamellar antigorite from Varenna Valley outcrop (Atg-5); h) massive prismatic tremolite from Campolungo (Trm-3). Field images of antigorite and tremolite samples embedded in their host rocks are reported in Supplementary Materials (S1).

fibrosity, based on the percentage of EMP. The resulting regression lines and coefficients are reported in Supplementary Materials S6.

4. Discussion

The presented analytical approach, tested on a comprehensive set of fibrous to lamellar/prismatic minerals, showed that the two parameters forming the basis to quantitatively discriminate between asbestos-like morphology from non-asbestos morphology are

– the percentage of EMP at max grinding time (20 min time; elevation in y axis in Fig. 4), after a controlled and reproducible mechanical stress (milling), namely $EMP_{20}\%$;
– the ability to limit the variation of EMP% with milling time up to 20 min (slope, S = ΔEMP%/milling time in minutes). (Supplementary Materials S6).

Antigorite and tremolite samples subjected to increasing and controlled mechanical stress exhibited four distinct morphological scenarios, as illustrated in Fig. 5. The position of the axes delimiting the four scenarios was determined through a maximum-margin

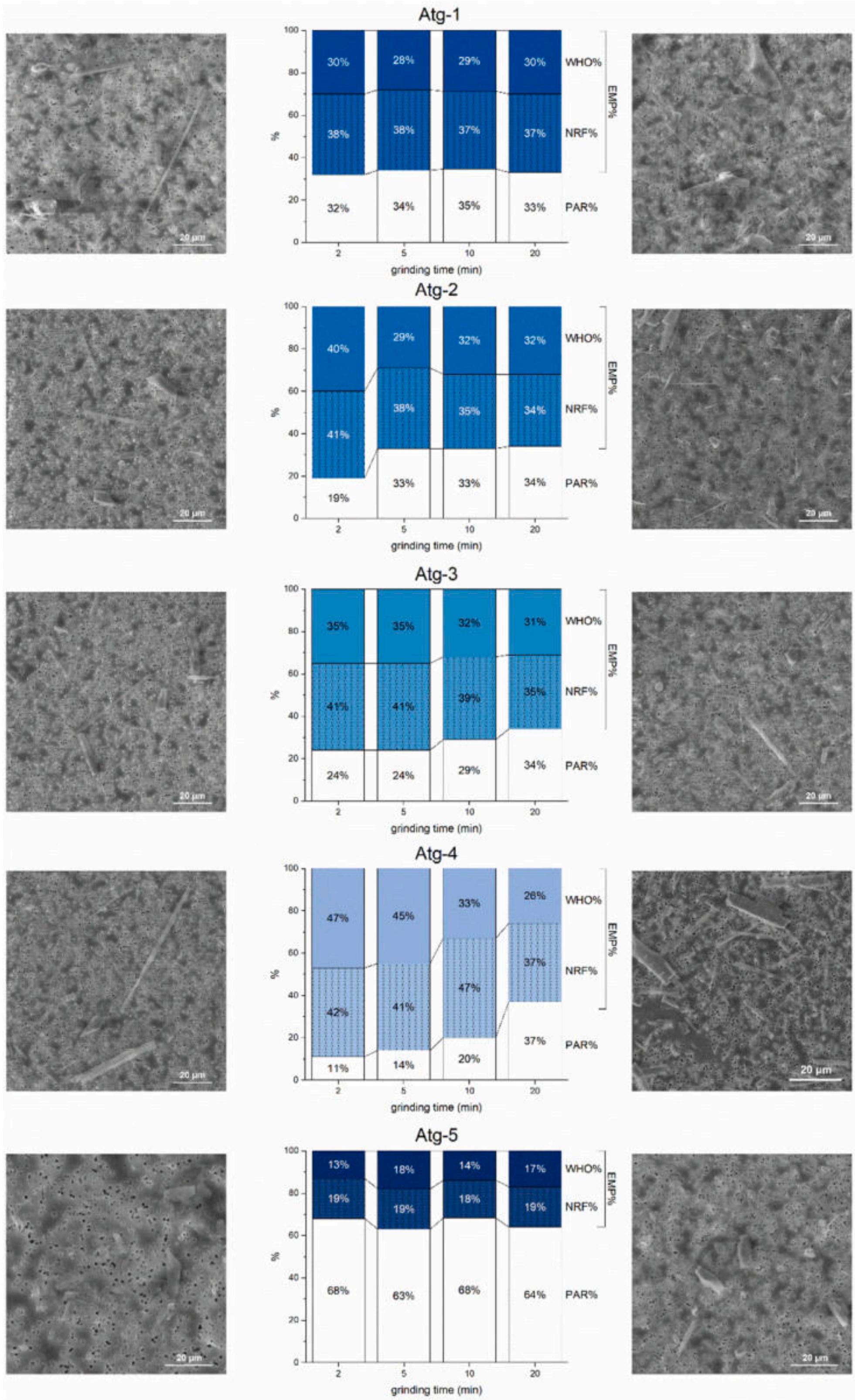

Fig. 3. Particle and fibre size distribution of antigorite (blue), tremolite (green), and non-asbestos fibre (MMVF) and lamellar talc (grey) samples after grinding at 2, 5, 10, and 20 min by optical and electron microscopies. Stacked column charts show the % variation of particles (AR <3; PAR% in white), non-respirable fibres (AR >3, L >5 µm, W >3 µm, NRF% in dotted colour), and WHO fibres (AR >3, L >5 µm, W <3 µm; WHO% in full colour) increasing the grinding time. The number of objects measured is reported in Supplementary Material S3. Representative SEM images illustrate the morphology for endpoint grinding times (t_2 on the left and t_{20} on the right) of each sample.

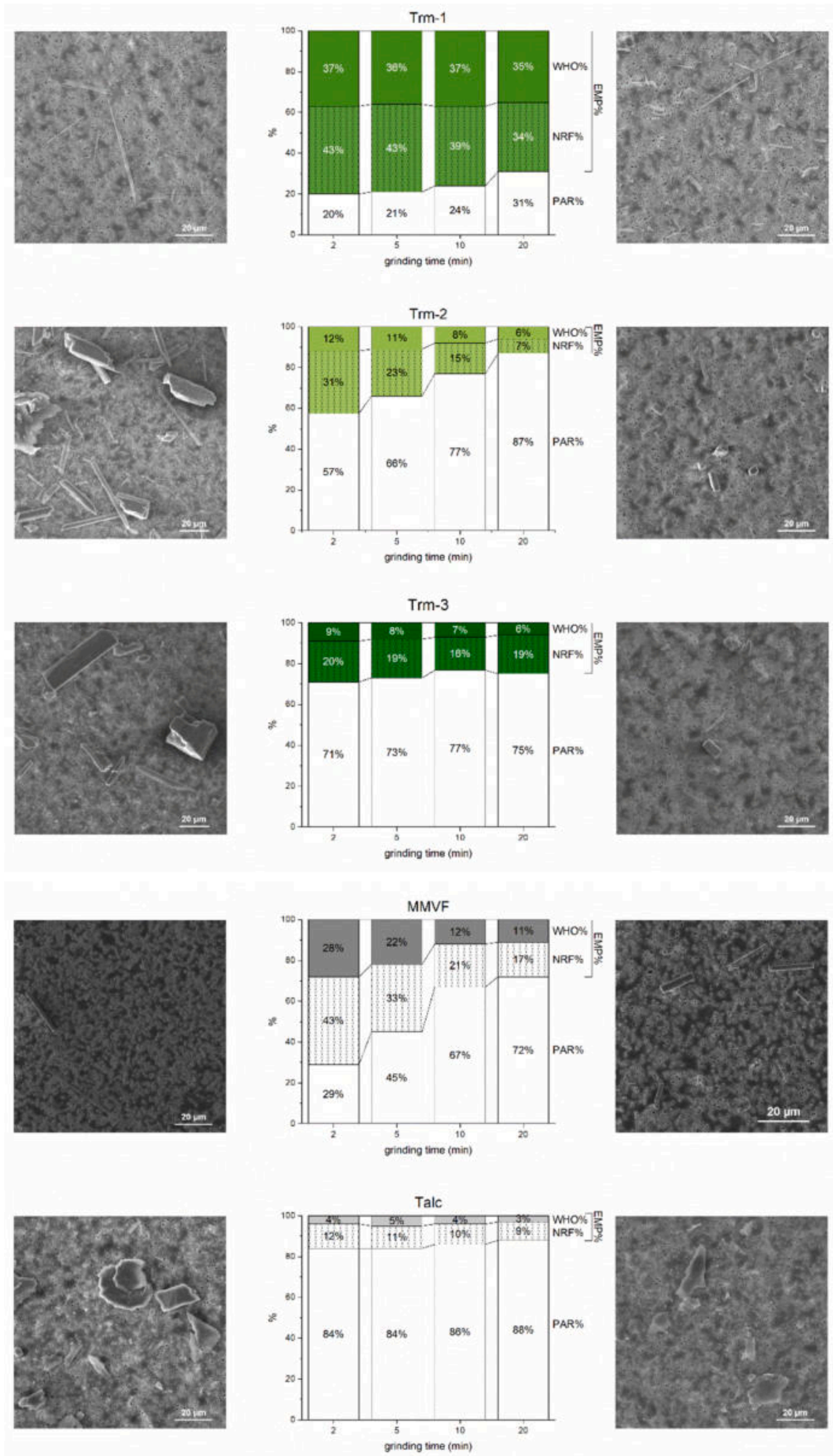

Fig. 3. (*continued*).

optimization procedure. Briefly, the vertical and horizontal axes were positioned to maximize the minimum distance between all data points and the nearest axis, thereby placing the boundaries in regions of lowest data density and avoiding arbitrary or data-cutting partitions. In cases of equivalent solutions, the horizontal axis was further optimized to maximize the separation along the y-dimension. Following this approach, the two axes delimiting the four scenarios were identified at $EMP_{20}\% = 49.5\%$ and $S = -1.05$. For practical reasons, the values were rounded to the nearest unit. Full details of the algorithm and implementation are provided in Supplementary Materials S7. The four

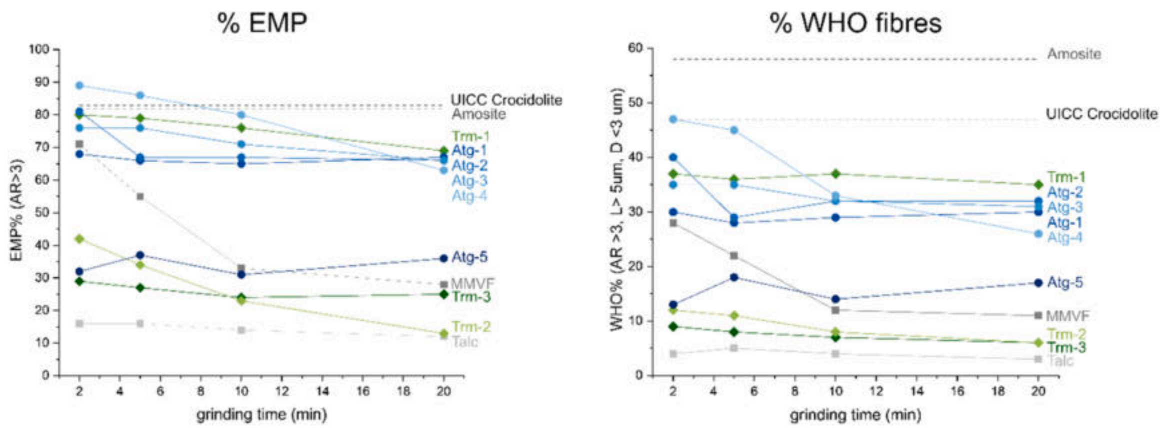

Fig. 4. Fibrosity behaviour of fibrous-to-lamellar/prismatic antigorite and tremolite samples subjected to increasing mechanical stress (grinding). Line graphs depict the progression of EMP% (on the left) and WHO% (on the right) increasing the milling time (t_2, t_5, t_{10}, and t_{20}). Non-asbestos fibres MMVF and lamellar talc were added for comparison. UICC crocidolite and amosite, derived from previously processed commercial asbestos materials, were not further milled and their EMP% and WHO% values are shown as dashed horizontal reference lines.

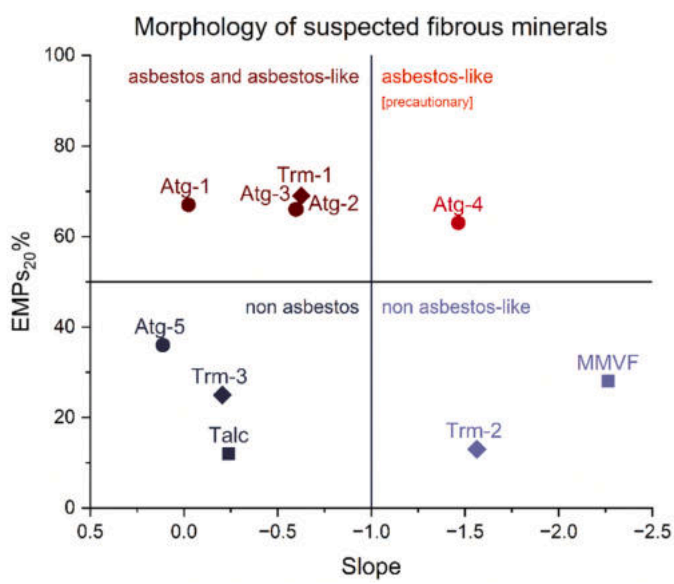

Fig. 5. Morphological classification of suspected fibrous minerals using the Fibrosity parameter F_p. The scatter plot with quadrant classification groups antigorite (circle) and tremolite (diamonds) based on morphometry at the endpoint milling time (EMP_{20}%) and the stability of EMP% under mechanical processing (slope). Morphology is classified into four morphological scenarios: asbestos and asbestos-like (dark-red, upper left quadrant), asbestos-like [precautionary] (red, upper right quadrant), non asbestos-like (violet, bottom right quadrant), and non-asbestos (dark-blue, bottom left quadrant).

scenarios calculated are:

1. Fibrous samples preserved their fibrosity, defined by $EMP_{20}\% > 50\%$ and $S > -1$, and fall within the morphometric parameters of regulated asbestos (e.g., UICC crocidolite, amosite). These samples (Fig. 5, dark-red region in the upper left quadrant) exhibit an asbestos (Trm-1) or an asbestos-like morphology (Atg-1, Atg-2, Atg-3);
2. Fibrous samples partially preserved their fibrosity, defined by $EMP_{20}\% > 50\%$ and $S < -1$, and ranked in the morphometry of asbestos-like to fibrous minerals. Supporting a precautionary distinction based on EMP content ($EMP_{20}\% > 50$), these samples (Fig. 5, red region in the upper right quadrant) may be ascribed to asbestos-like morphology (Atg-4);
3. Fibrous samples lost their fibrosity, defined by $EMP_{20}\% < 50\%$ and an $S < -1$, and ranked in the morphometric parameters of non asbestos-like fibres (e.g., MMVF). Although these samples (Fig. 5, violet region in the bottom right quadrant) show an elongated habit, they do not exhibit an asbestos-like morphology. Fibrous minerals can lose their fibrosity (Trm-2; [73]) and fall in the morphometric parameters of non asbestos-like morphology (MMVF);
4. Massive lamellar/prismatic samples preserved their prismatic/lamellar habit, defined by $EMP_{20}\% < 50\%$ and $S > -1$, and ranked in the morphometric parameters of non-asbestos (e.g., talc). These samples (Fig. 5, dark-blue region in the bottom left quadrant) exhibit a non-asbestos morphology (Atg-5, Trm-3).

Application of the Fibrosity parameter F_p to suspected asbestos-like minerals enables a quantitative, science-based discrimination between asbestos and asbestos-like and non-asbestos minerals, overcoming the subjective perceived fibrosity at the macroscopic scale. In some cases, the macroscopic morphology of centimetric or millimetric elongated fibres may recall the high aspect ratio characteristics of asbestos-like minerals. This study demonstrates that microscopic behaviour can differ significantly within fibrous to lamellar/prismatic specimens that belong to the same mineral species (e.g., tremolite). These aspects produce fragmentation patterns that generate particles and fibres in a very different dimensional range [43].

A flow-chart is proposed to guide laboratory analysts through a step-by-step evaluation of asbestos and asbestos-like morphology in suspected fibrous minerals. As illustrated in Fig. 6, the process begins with the assessment of the EMP% at the maximum endpoint of grinding (EMP_{20}%), followed by evaluating the ability to maintain a constant EMP%, expressed by the slope of the linear regression line.

If EMP_{20}% is greater than 50%, the analysis proceeds to the linear regression evaluation.

- If the slope is greater than −1, samples are assigned to asbestos and asbestos-like morphology (Fig. 6, dark-red box). This suggests a strong morphological similarity to asbestos in terms of crystal habit and size distribution. The presence of these samples in natural sites may require further regulatory and geological hazard consideration.
- If the slope is less than −1, samples can be assigned to the morphological group of asbestos-like [precautionary] (Fig. 6, red box), indicating that while they tend to lose their fibrosity increasing the mechanical stress, their high EMP content warrants a precautionary classification.

If EMP_{20}% is less than 50%, the analysis also proceeds to the linear

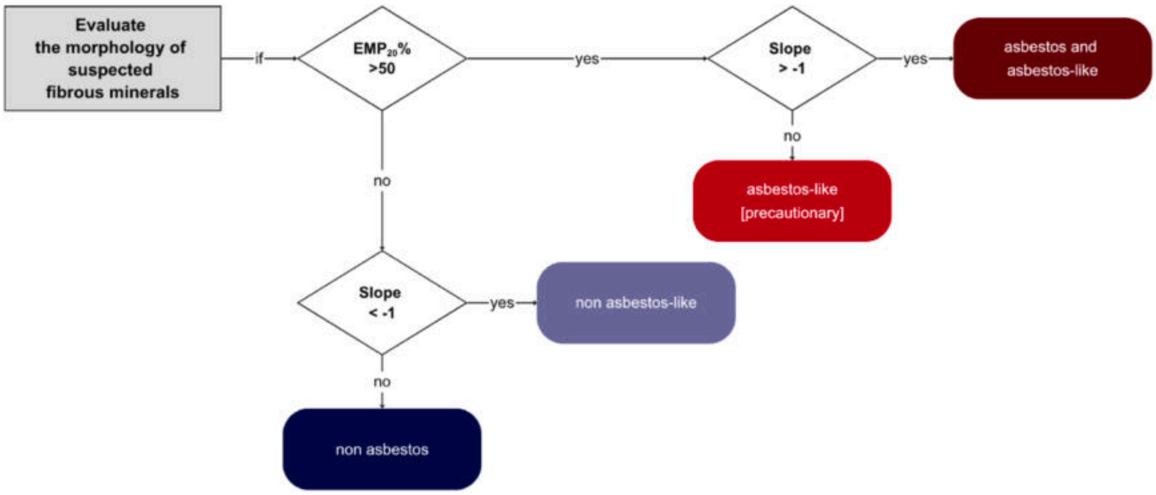

Fig. 6. The Fibrosity Parameter (F_p). Flow chart outlining the analytical protocol for assessing the potential asbestos-like morphology of suspected fibrous minerals.

regression evaluation.

- If the slope is less than −1, samples are assigned to the non asbestos-like morphology (Fig. 6, violet box), indicating a non negligible content of elongated particles that do not meet the criteria for EMP counting. The steep negative slope indicates that prolonged and intense mechanical stress (e.g., dry micronization) can cause the cleavage of elongated particles and fibres, preferentially reducing their length, resulting in isometric particles. This process has been considered for the inertization processing of fibrous minerals, as industrial sepiolite [74,75];
- If the slope is greater than −1, samples belong to the morphological classification of non-asbestos (Fig. 6, dark-blue box), indicating no significant resemblance to asbestos fibres in terms of particle habit or dimensional distribution.

The F_p evaluation scheme provides a robust and reproducible tool that laboratories can readily adopt for the screening and monitoring of suspected fibrous minerals. By enabling objective and quantitative evaluations, F_p complements traditional morphological assessments. This approach aims to offer a balanced and practical framework for identifying fibrous minerals that may pose a hazard, particularly in natural sites affected by infrastructure works. Notably, the inclusion of a precautionary category will support analytical judgment when particle features do not clearly align with established morphological classifications. Furthermore, the F_p approach could be integrated into current and future toxicity prediction models—such as the Fibre Toxicity Potential Index (FTPI)—and other quantitative frameworks aimed at assessing fibre toxicity.

Although F_p provides a robust quantitative descriptor of asbestos-like morphology, the use of the parameter has also limitations. F_p does not account for physicochemical and mineralogical parameters governing fibre toxicity, such as surface reactivity and solubility. Moreover, F_p does not estimate the abundance, dimensions, or release of airborne fibres from rocks under natural or anthropogenic disturbance, which is a parameter that is currently under investigation. The EMP% after milling and slope threshold values proposed ($EMP_{20}\% > 50\%$ and $S > -1$) were derived from the current dataset and should be validated across a broader range of NOA (e.g., erionite, glaucophane, winchite) from different NOA-bearing outcrops. Therefore, F_p should be interpreted as a morphological screening tool for suspected fibrous minerals and not as a stand-alone predictor of pathogenicity.

5. Conclusions

Asbestos toxicity has been strongly linked to the high aspect ratio and persistence of their mineral particles under mechanical stress. Since several NOA (e.g., fluoroedenite, erionite, and winchite) share toxic characteristics with asbestos, the development of robust and quantitative tools to assess asbestos-like morphology of suspected fibrous minerals is strongly warranted. In this work, we introduced the Fibrosity parameter (F_p), a two-dimensional and experimentally accessible approach based on the combination of EMP content after standardized milling ($EMP_{20}\%$) and its variation with increasing mechanical stress. This work proposes an innovative approach to morphologically discriminate asbestos and asbestos-like from non-asbestos minerals, namely on the ability to preserve high aspect ratio particles during progressive fragmentation. Among the investigated samples, fibrous antigorite and tremolite specimens exhibiting high EMP contents after milling (>50% at t = 20 min) and negligible variation of EMP% (ΔEMP %/ milling time > −1) were classified as asbestos or asbestos-like morphology, showing behaviour comparable to UICC crocidolite and amosite standards. In contrast, lamellar and prismatic samples, as well as non-asbestos references (talc and MMVF), displayed low EMP contents (<50% at t = 20 min) and a marked decrease of EMP% with milling time, consistent with non-asbestos morphology. Notably, a tremolite sample (Trm-2) with a clearly elongated macroscopic morphology was classified as a non-asbestos-like morphology, demonstrating that macroscopic fibrosity is not a reliable proxy for asbestos-like behaviour and highlighting the discriminating power of F_p. By providing a quantitative and reproducible descriptor of fragmentation-driven fibrosity, F_p enables a non-subjective classification of mineral occurences and represents a practical screening tool for the assessment of NOA in complex geological settings. However, as F_p is based exclusively on morphometric parameters, it does not account for physicochemical determinants of fibre toxicity and should therefore be regarded as a complementary tool within a broader hazard assessment framework rather than as a stand-alone predictor of pathogenicity.

Statement of environmental significance

Elongate mineral particles (EMP) in nature may represent an environmental hazard because disturbance of bearing rocks during construction, quarrying, erosion or weathering can release respirable asbestos and asbestos-like fibres and pose a risk to humans and the environment. Yet current field and laboratory analysis rely on subjective morphological analysis and does not account for mineral potency to generate fibres. This study defines fibrosity, a parameter that quantifies whether a suspected hazardous EMP preserves asbestos-like high-aspect-ratio after standardized mechanical stress. The approach supports environmentally relevant screening of EMP-bearing sites, improves hazard classification before excavation or remediation, and helps target monitoring and risk-control measures to minerals most likely to generate hazardous asbestos-like fibres.

CRediT authorship contribution statement

Maria Rosaria Bruno: Formal analysis, Data curation. **Angelo Olori:** Methodology, Formal analysis, Data curation. **Francesco Turci:** Writing – review & editing, Supervision, Resources, Project administration, Funding acquisition, Conceptualization. **Maura Tomatis:** Investigation, Data curation. **Alessandro Cavallo:** Resources, Formal analysis. **Alessandro Pacella:** Writing – review & editing, Validation, Supervision, Project administration. **Jasmine R. Petriglieri:** Writing – review & editing, Writing – original draft, Methodology, Investigation, Data curation, Conceptualization. **Antonella Campopiano:** Writing – review & editing, Resources, Project administration. **Luca Barale:** Writing – original draft, Methodology, Investigation, Data curation, Conceptualization. **Elena Belluso:** Validation, Supervision, Resources. **Fabrizio Piana:** Validation, Supervision, Resources, Conceptualization. **Biagio Maria Bruni:** Methodology, Formal analysis. **Paolo Ballirano:** Validation, Supervision, Resources, Methodology. **Chiara De Giuli:** Investigation.

Declaration of Generative AI and AI-assisted technologies in the writing process

During the preparation of this work, the authors used ChatGPT, powered by the GPT-5.6 Thinking model (OpenAI), through the ChatGPT Edu service provided under the University of Turin institutional subscription, to improve the English language and readability of the manuscript. The authors reviewed and edited the output as needed and take full responsibility for the content of the published article.

Declaration of Competing Interest

The authors declare that they have no known competing financial interests or personal relationships that could have appeared to influence the work reported in this paper.

Acknowledgements

This work was funded by the INAIL - BRIC 2019 project (grant number ID 57.1). FT acknowledges support from the Project CH4.0 under the MUR program "Dipartimenti di Eccellenza 2023–2027" (CUP: D13C22003520001). The Authors thank Paolo Gentile for kindly providing the prismatic Campolungo tremolite sample, and Gianfranco Fioraso and Luca Ossella for kindly providing the field photographs of, respectively, the Sauze d'Oulx tremolite veins and the Campolungo tremolite-bearing rocks, shown in Supplementary Materials (S1). The owner of the Bracchiello abandoned quarry is acknowledged for allowing access to the site and sampling.

Appendix A. Supporting information

Supplementary data associated with this article can be found in the online version at doi:10.1016/j.jhazmat.2026.143415.

Data Availability

Data will be made available on request.

References

[1] Botta, S., Avataneo, C., Barale, L., Compagnoni, R., Cossio, R., Marcelli, I., Piana, F., Tallone, S., Turci, F., 2020. Petrofacies for the prediction of NOA content in rocks: application to the "Gronda di Genova" tunnelling project. Bull Eng Geol Environ 79, 185–204. https://doi.org/10.1007/s10064-019-01539-6.
[2] Gaggero, L., Sanguineti, E., Yus González, A., Militello, G.M., Scuderi, A., Parisi, G., 2017. Airborne asbestos fibres monitoring in tunnel excavation. J Environ Manag 196, 583–593. https://doi.org/10.1016/j.jenvman.2017.03.055.
[3] Hendrickx, M., 2009. Naturally occurring asbestos in eastern Australia: a review of geological occurrence, disturbance and mesothelioma risk. Environ Geol 57, 909–926. https://doi.org/10.1007/s00254-008-1370-5.
[4] Lee, R.J., Strohmeier, B.R., Bunker, K.L., Van Orden, D.R., 2008. Naturally occurring asbestos - a recurring public policy challenge. J Hazard Mater 153, 1–21. https://doi.org/10.1016/j.jhazmat.2007.11.079.
[5] Diogo, M.T., 2020. European legal framework related to underground mining and tunnelling concerning Commission Directive (EU) 2017/164, 31 January, establishing a fourth list of indicative occupational exposure limit values. Int J Min Sci Technol 30, 541–545.
[6] Boffetta, P., 1998. Health effects of asbestos exposure in humans: a quantitative assessment. Med Lav 89, 471–480.
[7] Noonan, C.W., 2017. Environmental asbestos exposure and risk of mesothelioma, 234–234 Ann Transl Med 5. https://doi.org/10.21037/atm.2017.03.74.
[8] WHO, ILOWHO/ILO joint estimates of the work-related burden of disease and injury, 2000-2016: global monitoring report; 2021.
[9] Biggeri, A., Pasetto, R., Belli, S., Bruno, C., Di Maria, G., Mastrantonio, M., Trinca, S., Uccelli, R., Comba, P., 2004. Mortality from chronic obstructive pulmonary disease and pleural mesothelioma in an area contaminated by natural fiber (fluoro-edenite). Scand J Work Environ Health 249–252.
[10] Scarselli, A., Marinaccio, A., Iavicoli, S., 2021. Ophiolitic outcrops, naturally occurring asbestos exposure and mortality risk from malignant mesothelioma in Calabria (Southern Italy). Public Health 195, 57–60.
[11] Vignaroli, G., Ballirano, P., Belardi, G., Rossetti, F., 2014. Asbestos fibre identification vs. evaluation of asbestos hazard in ophiolitic rock mélanges, a case study from the Ligurian Alps (Italy). Environ Earth Sci 72, 3679–3698. https://doi.org/10.1007/s12665-014-3303-9.
[12] Vignaroli, G., Rossetti, F., Belardi, G., Billi, A., 2011. Linking rock fabric to fibrous mineralisation: A basic tool for the asbestos hazard. Nat Hazards Earth Syst Sci 11, 1267–1280. https://doi.org/10.5194/nhess-11-1267-2011.
[13] Harper, M., 2008. 10th Anniversary Critical Review: Naturally occurring asbestos. J Environ Monit 10, 1394–1408. https://doi.org/10.1039/b810541n.
[14] Cardile, V., Lombardo, L., Belluso, E., Panico, A., Capella, S., Balazy, M., 2007. Toxicity and carcinogenicity mechanisms of fibrous antigorite. Int J Environ Res Public Health 4, 1–9. https://doi.org/10.3390/ijerph2007010001.
[15] Gazzano, E., Petriglieri, J.R., Aldieri, E., Fubini, B., Laporte-Magoni, C., Pavan, C., Tomatis, M., Turci, F., 2022. Cytotoxicity of fibrous antigorite from New Caledonia. Environ Res, 115046. https://doi.org/10.1016/j.envres.2022.115046.
[16] Sullivan, P.A., 2007. Vermiculite, respiratory disease, and asbestos exposure in Libby, Montana: Update of a cohort mortality study. Environ Health Perspect 115, 579–585. https://doi.org/10.1289/ehp.9481.
[17] Giordani, M., Ballirano, P., Pacella, A., Meli, M.A., Roselli, C., Di Lorenzo, F., Fagiolino, I., Mattioli, M., 2022. Another potentially hazardous zeolite from northern Italy: Fibrous Mordenite. Minerals 12, 627.
[18] Gualtieri, A.F., Zoboli, A., Filaferro, M., Benassi, M., Scarfì, S., Mirata, S., Avallone, R., Vitale, G., Bailey, M., Harper, M., 2021. Vitro toxicity of fibrous glaucophane. Toxicology 454, 152743.
[19] Comba, P., Gianfagna, A., Paoletti, L., 2003. Pleural Mesothelioma Cases in Biancavilla are Related to a New Fluoro-Edenite Fibrous Amphibole. Arch Environ Health Int J 58, 229–232. https://doi.org/10.3200/AEOH.58.4.229-232.
[20] Luce, D., Bugel, I., Goldberg, P., Goldberg, M., Salomon, C., Billon-Galland, M.-A., Nicolau, J., Quénel, P., Fevotte, J., Brochard, P., 2000. Environmental exposure to tremolite and respiratory cancer in New Caledonia: a case-control study. Am J Epidemiol 151, 259–265. https://doi.org/10.1093/oxfordjournals.aje.a010201.
[21] Baris, I., Artvinli, M., Saracci, R., Simonato, L., Pooley, F., Skidmore, J., Wagner, C., 1987. Epidemiological and environmental evidence of the health effects of exposure to erionite fibres: a four-year study in the cappadocian region of turkey. Int J Cancer 39, 10–17.
[22] Bruno, C., Tumino, R., Fazzo, L., Cascone, G., Cernigliaro, A., De Santis, M., Giurdanella, M.C., Nicita, C., Rollo, P.C., Scondotto, S., 2014. Incidence of pleural mesothelioma in a community exposed to fibres with fluoro-edenitic composition in Biancavilla (Sicily, Italy). Ann Ist Super Sanita 50, 111–118.
[23] Carbone, M., Emri, S., Dogan, A.U., Steele, I., Tuncer, M., Pass, H.I., Baris, Y.I., 2007. A mesothelioma epidemic in Cappadocia: scientific developments and unexpected social outcomes. Nat Rev Cancer 7, 147–154.
[24] Goldberg, M., Luce, D., 2009. The health impact of nonoccupational exposure to asbestos: what do we know? Eur J Cancer Prev 18, 489–503.
[25] Temel, A., Gündoğdu, M.N., 1996. Zeolite occurrences and the erionite-mesothelioma relationship in Cappadocia, central Anatolia, Turkey. Miner Depos 31, 539–547.
[26] Cullinan, P., Muñoz, X., Suojalehto, H., Agius, R., Jindal, S., Sigsgaard, T., Blomberg, A., Charpin, D., Annesi-Maesano, I., Gulati, M., Kim, Y., Frank, A.L., Akgün, M., Fishwick, D., de la Hoz, R.E., Moitra, S., 2017. Occupational lung diseases: from old and novel exposures to effective preventive strategies. Lancet Respir Med 5, 445–455. https://doi.org/10.1016/S2213-2600(16)30424-6.
[27] Thives, L.P., Ghisi, E., Júnior, J.J.T., Vieira, A.S., 2022. Is asbestos still a problem in the world? A current review. J Environ Manag 319, 115716.

[28] Hyskaj, A., Weiszburg, T.G., Harman-Tóth, E., 2026. Asbestos legislation SITREP in the European Union: a mixed-methods analysis of parliamentary questions (1995–2024). Environ Sci Eur 38, 3.
[29] Baumann, F., Ambrosi, J.-P., Carbone, M., 2013. Asbestos is not just asbestos: an unrecognised health hazard. Lancet Oncol 14, 576–578.
[30] Erskine, B.G., Bailey, M., 2018. Characterization of asbestiform glaucophane-winchite in the Franciscan Complex blueschist, northern Diablo Range, California. Toxicol Appl Pharmacol 361, 3–13. https://doi.org/10.1016/j.taap.2018.09.020.
[31] Erskine, B.G., Bailey, M., 2021. Analysis of Baseline, Perimeter and Off-Site Air Monitoring Data from the Calaveras Dam Replacement Project, Fremont, California. Asbestos Other Elongate Mineral PartNew Contin Chall 21st Century 169–202.
[32] WHO, 1997. Determination of airborne fibre number concentrations. A recommended method, by phase-contrast optical microscopy (membrane filter method). Geneva.
[33] International Standard Organization, 2019. ISO 10312:2019 - Ambient air — Determination of asbestos fibres — Direct transfer transmission electron microscopy method.
[34] US-EPA, 1993. Method for the Determination of Asbestos in Bulk Building Material - Method 600/R-93/116. pp. 98.
[35] NIOSH, 2011. Asbestos fibers and other elongate mineral particles: State of the science and roadmap for research. Curr Intell Bull 62.
[36] Gualtieri, A.F., Leoncini, M., 2025. Comparison of the toxicity/carcinogenicity of regulated and unregulated mineral fibres using the Fibre Potential Toxicity Index (FPTI). J Hazard Mater, 139202.
[37] Weill D., 2023. The Monticello II Conference on Elongate Mineral Particles, Virginia, USA, 16-20 October 2017.
[38] Donaldson, K., Murphy, F.A., Duffin, R., Poland, C.A., 2010. Asbestos, carbon nanotubes and the pleural mesothelium: a review of the hypothesis regarding the role of long fibre retention in the parietal pleura, inflammation and mesothelioma. Part Fibre Toxicol 7, 5.
[39] Dodson, R.F., Atkinson, M.A.L., Levin, J.L., 2003. Asbestos fiber length as related to potential pathogenicity: a critical review. Am J Ind Med 44, 291–297.
[40] Korchevskiy, A.A., Wylie, A.G., 2022. Dimensional characteristics of the major types of amphibole mineral particles and the implications for carcinogenic risk assessment. Inhal Toxicol 34, 24–38.
[41] Wylie, A.G., Korchevskiy, A.A., 2023. Dimensions of elongate mineral particles and cancer: A review. Environ Res 230, 114688.
[42] Van Orden, D.R., 2023. Discriminant analysis of amphiboles: Additional considerations. Environ Res 230, 114579.
[43] Chatfield, E.J., 2023. Asbestiform fibers and cleavage fragments: conceptual approaches for differentiation in laboratory practice and data analysis. Environ Res 230, 114529.
[44] Siegrist, Jr.H.G., Wylie, A.G., 1980. Characterizing and discriminating the shape of asbestos particles. Environ Res 23, 348–361.
[45] Stanton, M.F., Layard, M., Tegeris, A., Miller, E., May, M., Morgan, E., Smith, A., 1981. Relation of Particle Dimension to Carcinogenicity in Amphibole Asbestoses and Other Fibrous Minerals. JNCI Journal National Cancer Institute 67 965975. https://doi.org/10.1093/jnci/67.5.965.
[46] Wylie, A.G., Virta, R.L., Russek, E., 1985. Characterizing and discriminating airborne amphibole cleavage fragments and amosite fibers: implications for the NIOSH method. Am Ind Hyg Assoc J 46, 197–201.
[47] Van Orden, D.R., Allison, K.A., Lee, R.J., 2008. Differentiating amphibole asbestos from non-asbestos in a complex mineral environment. Indoor Built Environ 17, 58–68.
[48] Berman, D.W., Crump, K.S., 2003. Final draft: technical support document for a protocol to assess asbestos-related risk. Prepared for Office of Solid Waste and Emergency Response. US Environmental Protection Agency, Washington, DC, 20460.
[49] Berman, D.W., Crump, K.S., 2008. A meta-analysis of asbestos-related cancer risk that addresses fiber size and mineral type. Crit Rev Toxicol 38, 49–73.
[50] Turci, F., Tomatis, M., Pacella, A., 2017. Surface and bulk properties of mineral fibres relevant to toxicity. European Mineralogical Union Notes in Mineralogy. Mineralogical Society, pp. 171–214.
[51] Gualtieri, A.F., Leoncini, M., Rinaldi, L., Zoboli, A., Di Giuseppe, D., 2021. WebFPTI: a tool to predict the toxicity/pathogenicity of mineral fibres including asbestos. Earth Sci Inform 14, 2401–2409.
[52] Davis, J.M., Addison, J., Bolton, R.E., Donaldson, K., Jones, A.D., Smith, T., 1986. The pathogenicity of long versus short fibre samples of amosite asbestos administered to rats by inhalation and intraperitoneal injection. Br J Exp Pathol 67, 415–430.
[53] Militello, G.M., Gaggero, L., La Maestra, S., 2021. Asbestiform amphiboles and cleavage fragments analogues: overview of critical dimensions, aspect ratios, exposure and health effects. Minerals 11, 525.
[54] La Maestra, S., Militello, G.M., Alberti, S., Benvenuti, M., Gaggero, L., 2025. Evaluation of the genotoxic and transformation potential induced by asbestos compared to cleavage fragments. Sci Rep 15, 3613.
[55] Militello, G.M., Sanguineti, E., Gonzàlez, A., Gaggero, L., 2020. Asbestos amphiboles: Effects of comminution on tremolite and actinolite regulated and unregulated fibres. Epis J Int Geosci 43, 909–918.
[56] Petriglieri, J.R., Capitani, G., Ballirano, P., Barale, L., Piana, F., Tomatis, M., Di Carlo, M.C., Gianchiglia, F., Campopiano, A., Olori, A., 2025. Naturally occurring asbestos in Southern italy: geological and mineralogical investigation of fibrous Antigorite from Calabrian serpentinites in view of its hazard assessment. Sci Total Environ 970, 178970.
[57] Gualtieri, A.F., 2017. Introduction. In: Gualtieri AF (ed) Mineral fibres: Crystal chemistry, chemical physical properties, biological interaction and toxicity. EMU Notes. European Mineralogical Union and the Mineralogical Society of Great Britain, Ireland, UK, pp. 1–15.
[58] IARC, 2012. Monographs on the Evaluation of Carcinogenic Risks to Humans. Arsenic, Metals. Fibres, and Dusts. A review of human carcinogens (Lyon, France).
[59] Meeker, G.P., Bern, A.M., Brownfield, I.K., Lowers, H.A., Sutley, S.J., Hoefen, T.M., Vance, J.S., 2003. The composition and morphology of amphiboles from the Rainy Creek complex, near Libby, Montana. Am Mineral 88, 1955–1969. https://doi.org/10.2138/am-2003-11-1239.
[60] Belluso, E., Cavallo, A., Halterman, D., 2017. Crystal habit of mineral fibres. In: Gualtieri AF (ed) Mineral fibres: Crystal chemistry, chemical physical properties, biological interaction and toxicity. EMU Notes. European Mineralogical Union and the Mineralogical Society of Great Britain, Ireland, UK, pp. 65–109.
[61] Pacella, A., Andreozzi, G., Nodari, L., Ballirano, P., 2019. Chemical and structural characterization of UICC crocidolite fibres from Koegas Mine, Northern Cape (South Africa). Period di Mineral 88, 297–306.
[62] Tomatis, M., Turci, F., Ceschino, R., Riganti, C., Gazzano, E., Martra, G., Ghigo, D., Fubini, B., 2010. High aspect ratio materials: role of surface chemistry vs. length in the historical "long and short amosite asbestos fibers. Inhal Toxicol 22, 984–998.
[63] TIMA (Thermal Insulation Manufacturers Association), 1991. Man-made Vitreous Fibers: Nomenclature, Chemical and Physical Properties. IPCS-WHO.
[64] Cadoppi, P., Camanni, G., Balestro, G., Perrone, G., 2016. Geology of the Fontane talc mineralization (Germanasca valley, Italian Western Alps). J Maps 12, 1170–1177.
[65] Petriglieri, J.R., Barale, L., Viti, C., Ballirano, P., Belluso, E., Bruno, M.R., Campopiano, A., Cannizzaro, A., Fantauzzi, M., Gianchiglia, F., 2023. From field analysis to nanostructural investigation: A multidisciplinary approach to describe natural occurrence of asbestos in view of hazard assessment. J Hazard Mater 457, 131754.
[66] Groppo, C., 2006. Asbestos hazard in Western Alps. Petrology, characterizations and quantitative determination of fibrous minerals in the asbestos-bearing serpentinites of the Piemonte Zone (Susa and Lanzo Valleys). Università di Torino.
[67] Bittarello E., Ciriotti M., 2014. Identificazione di alcuni minerali della Val d'Ala. Minerali in Val d'Ala. Associazione Amici del Museo "F. Eusebio"
[68] Mercolli, I., Skippen, G., Trommsdorff, V., 1987. The tremolite veins of Campolungo and their genesis. Schweiz Mineral und Petrogr Mitt 67, 75–84.
[69] Clarke, J., Gamble, J.F., Jones, J.W., Tobyn, M., Greenwood, R., Ingram, A., 2019. Alternative approach for defining the particle population requirements for static image analysis based particle characterization methods. Adv Powder Technol 30, 920–929.
[70] Turci, F., Avataneo, C., Botta, S., Marcelli, I., Barale, L., Tomatis, M., Cossio, R., Tallone, S., Piana, F., Compagnoni, R., 2020. New tools for the evaluation of asbestos-related risk during excavation in an NOA-rich geological setting. Environ & Eng Geosci 26, 113–120.
[71] Gy, P., 1998. Sampling for analytical purposes. John Wiley & Sons.
[72] IMA, 2022. IMA Working Group on "Asbestos, asbestiform minerals, and other respirable minerals that pose potential negative health risks" deliberations and recommendations. pp.7.
[73] Baietto, O., Diano, M., Zanetti, G., Marini, P., 2019. Grinding test on tremolite with fibrous and prismatic habit. Fibers 7, 52.
[74] Cornejo, J., Hermosin, M.C., 1988. Structural alteration of sepiolite by dry grinding. Clay Miner 23, 391–398.
[75] Paolini, V., Tomassetti, L., Segreto, M., Borin, D., Liotta, F., Torre, M., Petracchini, F., 2019. Asbestos treatment technologies. J Mater Cycles Waste Manag 21, 205–226.